Inorganic Chemistry

Article

pubs.acs.org/IC

Solid-State Ligand-Driven Light-Induced Spin Change at Ambient Temperatures in Bis(dipyrazolylstyrylpyridine)iron(II) Complexes

Kazuhiro Takahashi,[†] Yuta Hasegawa,[†] Ryota Sakamoto,[†] Michihiro Nishikawa,[†] Shoko Kume,[†] Eiji Nishibori,[‡] and Hiroshi Nishihara*[,†]

[†]Department of Chemistry, Graduate School of Science, The University of Tokyo, 7-3-1, Hongo, Bunkyo-ku, Tokyo, 113-0033 Japan

[‡]Department of Applied Physics, Nagoya University, Nagoya 464-8603, Japan

Supporting Information

ABSTRACT: We previously reported that an Fe^{II} complex ligated by two (*Z*)-2,6-di(1*H*-pyrazol-1-yl)-4-styrylpyridine ligands (**Z-H**) presented a solid state ligand-driven light-induced spin change (LD-LISC) upon one-way *Z*-to-*E* photoisomerization, although modulation of the magnetism was trivial at ambient temperatures (*Chem. Commun.* **2011**, *47*, 6846). Here, we report the synthesis of new derivatives of **Z-H**, **Z-CN** and **Z-NO_2**, in which electron-withdrawing cyano and nitro substituents are introduced at the 4-position of the styryl group to attain a more profound photomagnetism at ambient temperatures. **Z-CN** and **Z-NO_2** undergo quantitative one-way *Z*-to-*E* photochromism upon excitation of the charge transfer band both in acetonitrile and in the solid state, similar to the behavior observed for **Z-H**. In solution, these substituents stabilized the low-spin (LS) states of **Z-CN** and **Z-NO_2**, and the behavior was quantitatively analyzed according to the Evans equation. The photomagnetic properties in the solid state, on the other hand, cannot be explained in terms of the substituent effect alone. **Z-CN** displayed photomagnetic properties almost identical to those of **Z-H**. **Z-CN** preferred the high-spin (HS) state at all temperatures tested, whereas photoirradiated **Z-CN** yielded a lower $\chi_M T$ at ambient temperatures. The behavior of **Z-NO_2** was counterintuitive, and the material displayed surprising photomagnetic properties in the solid state. **Z-NO_2** occupied the LS state at low temperatures and underwent thermal spin crossover (SCO) with a $T_{1/2}$ of about 270 K. The photoirradiated **Z-NO_2** displayed a higher value of $\chi_M T$ and the modulation of $\chi_M T$ exceeded that of **Z-H** or **Z-CN**. **Z-NO_2·acetone**, in which acetone molecules were incorporated into the crystal lattice, further stabilized the LS state ($T_{1/2}$ > 300 K), thereby promoting large modulations of the $\chi_M T$ values (87% at 273 K and 64% at 300 K) upon *Z*-to-*E* photoisomerization. Single crystal X-ray structure analysis revealed that structural factors played a vital role in the photomagnetic properties in the solid state. **Z-H** and **Z-CN** favored intermolecular $\pi-\pi$ stacking among the ligand molecules. The coordination sphere around the Fe^{II} nucleus was distorted, which stabilized the HS state. In contrast, **Z-NO_2·acetone** was liberated from such intermolecular $\pi-\pi$ stacking and coordination distortion, resulting in the stabilization of the LS state.

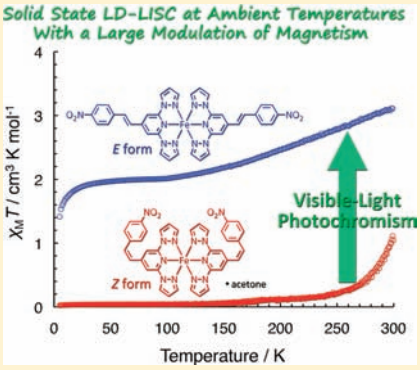

INTRODUCTION

Spin crossover (SCO)[1−4] is a phenomenon in which the spin state of a metal center switches between the low-spin (LS) and high-spin (HS) states under an external stimulus, such as temperature, pressure, or light. Octahedral first row transition metal complexes with electronic configurations of d^4-d^7 exhibit SCO. Light-induced excited spin state trapping (LIESST),[1−4] in which light-induced electronic transitions involve a change from the stable LS state to the metastable HS state below the thermal spin crossover temperature, has been extensively investigated. Light-controllable systems present tremendous advantages over systems controlled via other stimuli, including practical reversibility, controllability over the power supply, and selectivity with respect to the irradiation wavelength. The LIESST effects were first reported by Decurtins and co-workers in 1984 in the context of $[Fe^{II}(ptz)_6](BF_4)_2$ (ptz = 1-propyltetrazole).[5] LIESST is based on the photoexcitation of the stable LS ($S = 0$) state via d−d and metal-to-ligand charge transfer (MLCT) transitions, followed by trapping of the metastable HS ($S = 2$) state.

The thermal stability of the metastable HS state, which is often represented as a convenient observable parameter T(LIESST),[4,6−8] is central to the practical application of LIESST materials. LIESST phenomena have been primarily observed only under cryogenic conditions, and much effort has been devoted to increasing T(LIESST), for example, by using multidentate ligands[4,6−8] or intermolecular cooperative effects, such as $\pi-\pi$ interactions[9−12] and hydrogen bonding.[13−16] Despite significant efforts, the highest value of T(LIESST) yet achieved, 132 K,[17−19] is substantially below ambient temperatures.

A new strategy for achieving photomagnetic switching, that is, ligand-driven light-induced spin change (LD-LISC), was first

Received: January 5, 2012
Published: April 11, 2012

   dx.doi.org/10.1021/ic300030b | *Inorg. Chem.* 2012, 51, 5188−5198

proposed by Zarembowitch et al.[20] The prerequisite for LD-LISC is that ligand molecules contain organic photochromics, the photoisomerization of which affects the spin equilibrium between the LS and HS states. The advantage of LD-LISC over LIESST is that the former is potentially available even at ambient temperatures: The lifetimes of metastable states at ambient temperatures are far longer in the former than in the latter.

The LD-LISC systems reported thus far have been demonstrated only in solution or polymer media[21−23] because the photoisomerization of organic photochromics was considered to require a certain degree of free volume. Recently, solid-state LD-LISC has been pursued with mixed results. Boillot and co-workers synthesized an Fe^{II} complex containing a pyridine-incorporated dithienylethene ligand, only to find no photomagnetic effects upon photoisomerization of the dithienylethene moiety.[24] Boillot and co-workers also investigated $Fe^{II}(stpy)_4(NCSe)_2$ (stpy = 4-styrylpyridine).[25] In this system, the authors identified a one-way *Z*-to-*E* photochromism in the solid state. Photoisomerization resulted in LD-LISC, although it did not affect $\chi_M T$ beyond 250 K; both the *E*- and *Z*-isomers were present solely in the HS state ($S = 2$).

We independently reported another stilbenoid Fe^{II} complex, ***Z*/*E*-H**, containing two 2,6-di(1*H*-pyrazol-1-yl)-4-styrylpyridine) ligands (Scheme 1).[26] The *Z*-form underwent a visible light one-way *Z*-to-*E* photochromism to the *E*-form in the solid state. Tridentate ligand 2,6-di(1*H*-pyrazol-1-yl)-4-pyridine induced a ligand field suitable for thermal SCO at ambient temperatures.[27] ***Z*-H** occupied the HS state below 300 K, whereas ***E*-H** was in equilibrium between the HS and LS states over this temperature range. The $\chi_M T$ values varied from 3.6 cm^3 K mol^{-1} to 3.1 cm^3 K mol^{-1} upon *Z*-to-*E* photoisomerization at 300 K. ***Z*/*E*-H**, therefore, is the first system to display solid state LD-LISC at ambient temperatures, although the photomagnetic changes were not large.

Scheme 1. Photoisomerization from the *Z*-Form to the *E*-Form upon Visible Light (λ > 420 nm) Irradiation in Fe^{II} Complexes Studied[a]

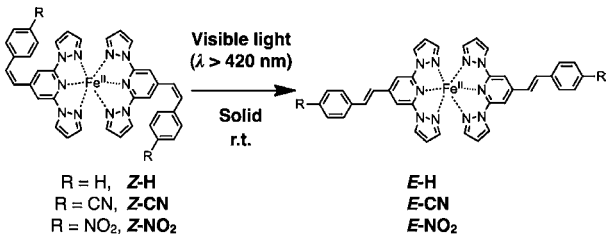

[a]Counter anions are omitted.

This work has primarily served to improve the amplitude of photomagnetic modulation in an LD-LISC system. To this end, the influences of substituents on the stilbenoid ligand were employed to tune the ligand field properties. Electron-withdrawing substituents, nitro and cyano groups, were introduced to reduce the energy of the π^* orbital in the 2,6-di(1*H*-pyrazol-1-yl)-4-pyridine ligand, which promoted π-back-donation, a stronger ligand field, and more stabilization of the LS state.[28,29] We also expected that the substituents on the stilbenoid ligand might tune the intermolecular interactions in the solid state to significantly influence the SCO behavior.[30] In solution, the electronic substituent effects solely improve the stability of the LS state, as predicted by the Hammett equation. In the solid state, intermolecular interactions play a vital role. ***Z*-CN**, which features intermolecular $\pi-\pi$ stacking just as ***Z*-H**, exhibits a little decrease in $\chi_M T$ in the solid state upon *Z*-to-*E* photoisomerization at ambient temperatures. In contrast, ***Z*-NO_2·acetone**, which does not feature intermolecular interactions in the crystalline state, presents a counterintuitive LS→HS transition with large variations in the $\chi_M T$ values, even at ambient temperatures (**acetone**: a crystal solvent).

RESULTS AND DISCUSSION

Syntheses. The synthetic details are described in the Experimental Section. The essence of these procedures is briefly introduced here. The stilbene-conjugated ligands were synthesized by Wittig reactions between 2,6-di(1*H*-pyrazol-1-yl)isonicotinaldehyde and the corresponding phosphonium bromides such that the ligands were obtained as mixtures of the *E*- and *Z*-isomers. These isomers were successfully isolated by alumina column chromatography, and the *E*-*Z* configuration was determined based on the *J*-coupling value between the two protons on the ethylene moiety in ^1H NMR spectra. These isomers of the ligands were used to prepare, separately, the corresponding complexes with the *E*-and *Z*-configurations. The complexes were identified using ESI-TOF mass and FT-IR spectroscopies, and elemental analysis. The complexes with *E*- and *Z*-configuration were characterized by single-crystal X-ray diffraction (XRD) analysis. A detailed discussion of the crystal structures of *E*- and *Z*-forms is described in a later section.

1. Photoisomerization Behavior. UV−vis Spectra of the Z-Isomers. Figure 1 shows the UV−vis spectra of ***Z*-H**, ***Z*-CN**, and ***Z*-NO_2** in acetonitrile. The strong absorption band at 320 nm was assigned to a mixture of $\pi-\pi^*$ and $n-\pi^*$ transitions of the 2,6-di(1*H*-pyrazol-1-yl)-4-styrylpyridine ligands,[31] whereas the weak and broad absorption band at 450 nm was attributed to metal-to-ligand charge transfer (MLCT) band. This MLCT band was slightly red-shifted in ***Z*-CN** and ***Z*-NO_2** compared to ***Z*-H**, suggesting that the introduction of electron-withdrawing nitro and cyano groups lowered the ligand π^* orbital energy level. Such effects were expected to increase the ligand field splitting and stabilize the LS state.

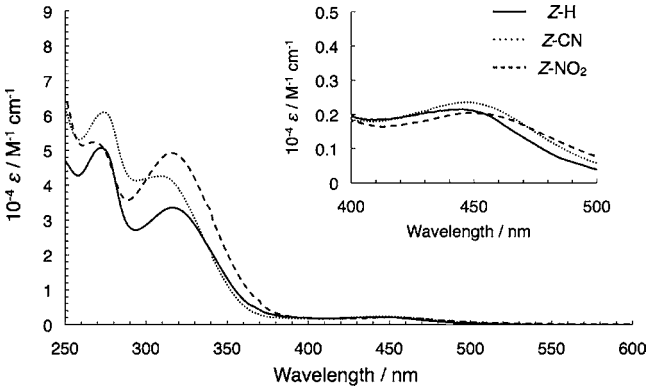

Figure 1. UV−vis spectra of ***Z*-H**, ***Z*-CN**, and ***Z*-NO_2** in acetonitrile at 295 K. The inset shows an expanded view of the MLCT absorption region.

Photoisomerization in Solution. In the previous communication, we reported that ***Z*-H** exhibited complete one-way *Z*-to-*E* photoisomerization in acetone at room temperature upon irradiation with 436 nm light, which corresponded to excitation of the MLCT band.[26] ***Z*-H** displayed a similar photoresponse in

dx.doi.org/10.1021/ic300030b | Inorg. Chem. 2012, 51, 5188−5198

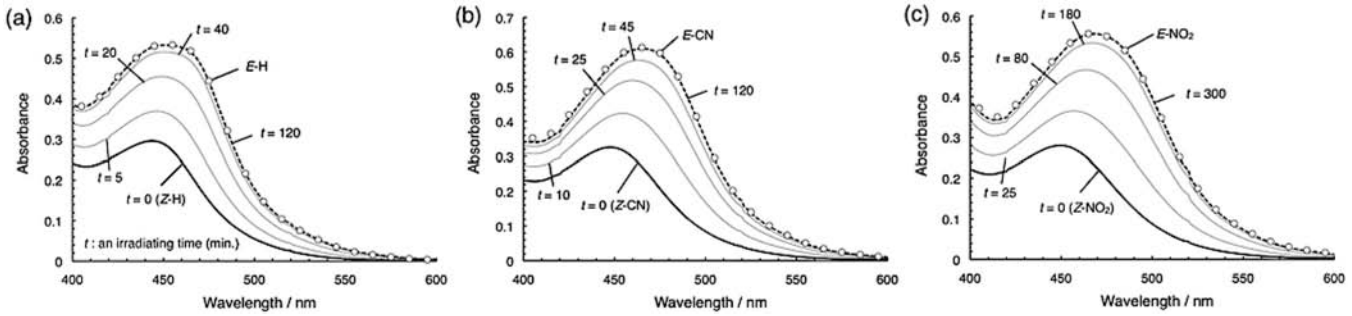

Figure 2. UV−vis spectral changes of (a) **Z-H**, (b) **Z-CN**, and (c) **Z-NO$_2$** in acetonitrile upon irradiation with 436 nm light. The spectra of the corresponding *E*-form complexes are indicated by black circles, and the concentrations of the complexes were 1.0×10^{-4} M.

acetonitrile at room temperature (Figure 2a). Upon irradiation with 436 nm light, the absorption intensity of the MLCT band increased and its absorption maximum shifted toward the red. The resultant spectrum matched that of the synthesized ***E*-H**. An acetonitrile solution of ***E*-H** did not reveal spectral changes upon excitation of the MLCT band. These results indicate that one-way *Z*-to-*E* photoisomerization proceeded quantitatively in acetonitrile. Similarly, photoirradiation of **Z-CN** and **Z-NO$_2$** with 436 nm light resulted in one-way *Z*-to-*E* photoisomerization (Figure 2b, 2c). The molar extinction coefficient of the MLCT band of the LS Fe^{II} complexes far exceeded that of HS complexes.[32] Therefore, the spectral changes that accompanied the *Z*-to-*E* photoisomerization in our complexes suggested that the fraction of the LS species increased in the *E*-forms. Note that this system underwent spectral changes that were unlike those observed for Fe^{II}(stpy)$_4$(NCSe)$_2$. In that system, the intensity of the MLCT band was reduced upon *Z*-to-*E* photoisomerization, and the authors determined that both isomers occupied the HS state at room temperature.[25] Our system may be better suited for LD-LISC at ambient temperatures in the solid state.

Photoisomerization in a KBr Pelletized Sample. The one-way *Z*-to-*E* photoisomerization was investigated using FT-IR spectroscopy (KBr pellet). KBr pelletized samples of each complex were irradiated with visible light (λ > 420 nm) to excite the MLCT absorption band, as in solution. Upon irradiation, the color changed from yellow to dark orange or red in all complexes. The photoirradiated samples were the same color as the synthesized *E*-forms (Figure 3). The FT-IR spectrum of the photoirradiated **Z-NO$_2$** also agreed with that of ***E*-NO$_2$**, and the characteristic **Z-NO$_2$** peaks disappeared (Supporting Information, Figure S1). In **Z-CN**, a peak derived from the C−H out-of-plane bending of the alkenyl moieties[33,34] at 974 cm^{-1} was shifted to 971 cm^{-1}, as in other stilbene-attached derivatives,[35,36] including **Z-H**,[26] upon *Z*-to-*E* photoisomerization. These results suggest that the one-way *Z*-to-*E* isomerization by visible light irradiation was active in the solid medium, and introduction of cyano and nitro substituents did not alter the photoresponse.

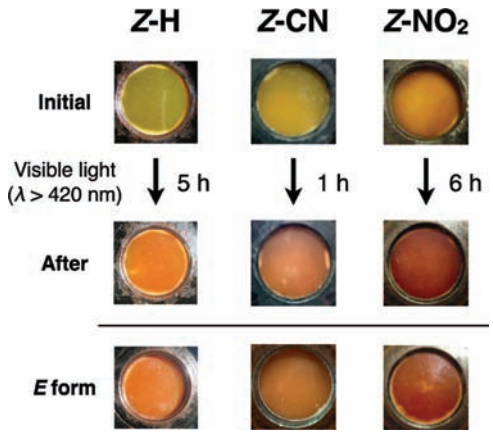

Figure 3. Color changes of the KBr pelletized samples of **Z-H**, **Z-CN**, and **Z-NO$_2$** upon irradiation with visible light (λ > 420 nm) for 5 h in **Z-H**, 1 h in **Z-CN**, and 6 h in **Z-NO$_2$**.

Photoisomerization in the Crystalline State. Bulk microcrystalline samples of **Z-H**, **Z-CN**, **Z-NO$_2$**, and **Z-NO$_2$·acetone** were irradiated with visible light (λ > 420 nm) for a few days until they presented significant color changes (Figure 4). For example, **Z-CN** turned from yellow to dark orange. The *E*/*Z* ratios in the photostationary state (PSS) were estimated based on the FT-IR spectra (KBr pelletized state) and the UV−vis spectra of the microcrystals in the PSS, dissolved in acetonitrile. Both spectroscopic studies revealed a conversion ratio from the *Z*-form to the *E*-form of no less than 88% (Figure 5). Further irradiation did not influence the *E*/*Z* ratios, presumably because of the inner filter effects of the crystalline solid.[37] Powder XRD analysis indicated that the photoproducts, which were dominated by the *E*-forms, as shown above, lost their crystallinity (Supporting Information, Figure S2).

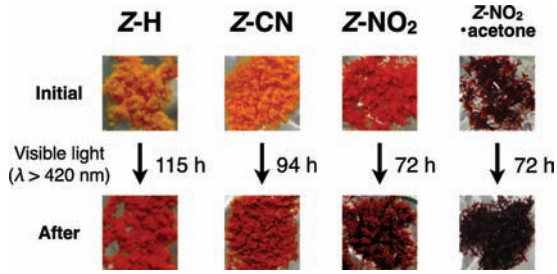

Figure 4. Color changes of the microcrystalline **Z-H**, **Z-CN**, **Z-NO$_2$**, and **Z-NO$_2$·acetone** upon irradiation with visible light (λ > 420 nm) for 115 h in **Z-H**, 94 h in **Z-CN**, and 72 h in **Z-NO$_2$** and **Z-NO$_2$·acetone**.

2. LD-LISC Behavior. Thermal SCO in Acetone Solutions. The magnetization of the *Z*-form in solution was estimated using the Evans method in acetone-d_6.[38] The measurements were performed over the temperature range 220−290 K. All complexes showed thermal SCO over this temperature range, and the temperature dependence of the resultant $\chi_M T$ values was fit using the van't Hoff equation to calculate the thermodynamic parameters of thermal SCO (see Experimental

dx.doi.org/10.1021/ic300030b | *Inorg. Chem.* 2012, 51, 5188−5198

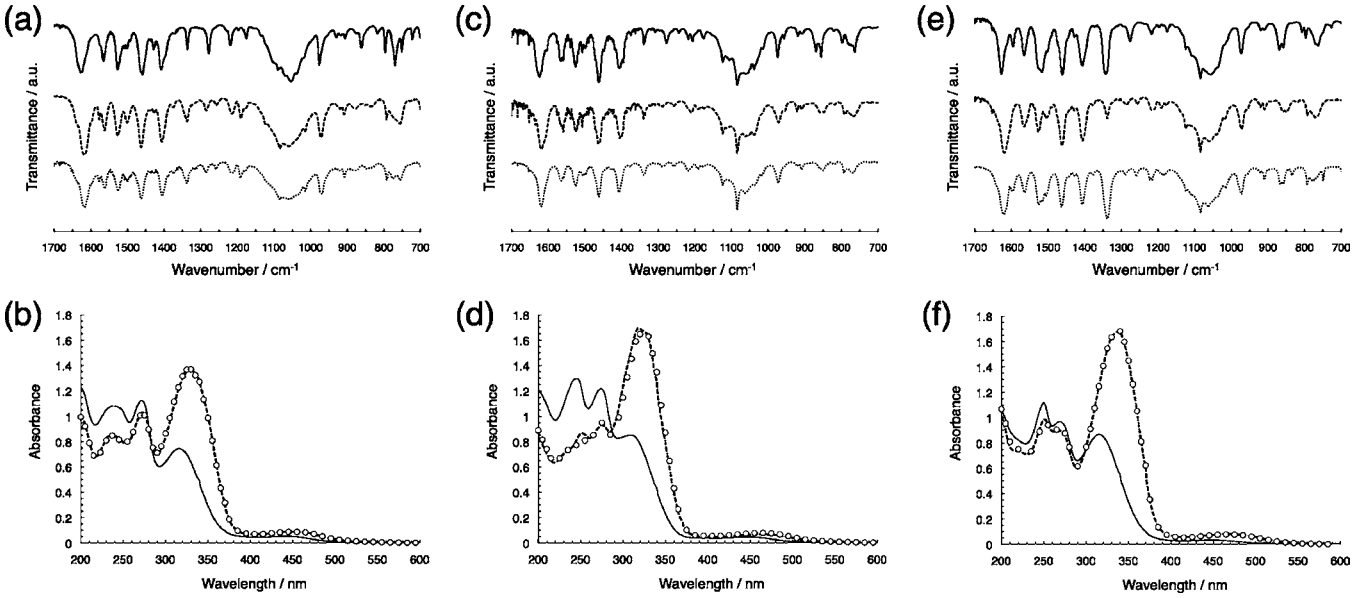

Figure 5. FT-IR spectra of photoproducts of (a) **Z-H**, (c) **Z-CN**, and (e) **Z-NO_2** in the microcrystalline solid by irradiation with visible light (broken lines), together with those of pure *Z*-(solid lines) and *E*-isomers (dotted lines). UV−vis spectra of photoproducts of (b) **Z-H**, (d) **Z-CN**, and (f) **Z-NO_2** in acetonitrile (broken lines), together with those of pure *Z*-isomers (solid lines). The concentration of each complex was 2.0×10^{-5} M. The simulated UV−vis spectra (represented as circles) indicated by the circles corresponded to the mixture of (b) **Z-H** and ***E*-H** in a ratio of 12:88, (d) **Z-CN** and ***E*-CN** in a ratio of 8:92, and (f) **Z-NO_2** and ***E*-NO_2** in a ratio of 12:88.

Section for the details). Resultant van't Hoff plots for three complexes are shown in Figure 6 with the regression lines,

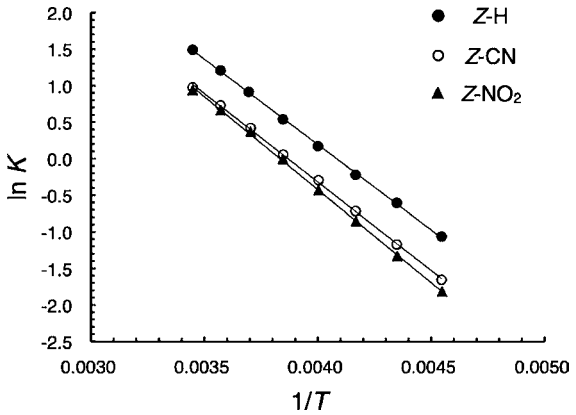

Figure 6. van't Hoff plots for **Z-H**, **Z-CN**, and **Z-NO_2** in acetone-d_6. The regression lines are indicated by the solid lines.

which afford the thermodynamic parameters listed in Table 1 and the crossover temperatures $T_{1/2}$ of 245 K, 259 K, 261 K for **Z-H**, **Z-CN**, and **Z-NO_2**, respectively. The van't Hoff model reproduced well the experimental results (Figure 7). The significant increase in $T_{1/2}$ in **Z-CN** and **Z-NO_2** compared to **Z-H** suggested stabilization of the LS state by the electronic effect

Table 1. SCO Temperatures and Thermodynamic Parameters for Z-H, Z-CN, and Z-NO_2, Determined by the Evans Method

	$T_{1/2}$/K	ΔH/kJ mol^{-1}	ΔS/J mol^{-1} K^{-1}
Z-H	245	19.4	79
Z-CN	259	20.1	78
Z-NO_2	261	21.1	81

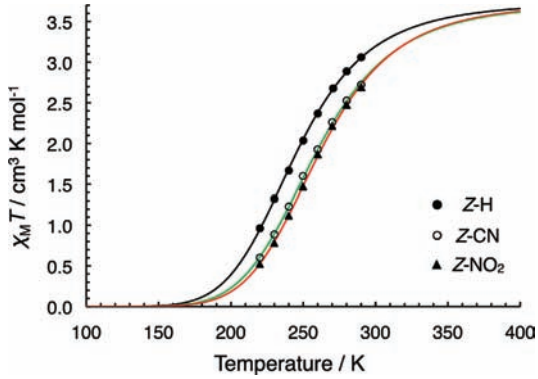

Figure 7. $\chi_M T$ vs T plots of **Z-H** (filled circle), **Z-CN** (open circle), and **Z-NO_2** (triangle) in acetone-d_6, determined using the Evans method. van't Hoff models using thermodynamic parameters in Table 1 are indicated by the solid lines (a black line for **Z-H**, a green line for **Z-CN**, and a red line for **Z-NO_2**).

of the electron-withdrawing substituents. This conclusion was quantitatively supported by the $T_{1/2}$-Hammett constant σ_p plots (Figure 8).[39] We note that the $\chi_M T$ values for the *E*-forms were not acquired using the Evans method because of the low solubility of these forms in solvents.

LD-LISC Behavior in the Solid State. Variable-temperature magnetic susceptibility measurements for **Z-H**, **Z-CN**, **Z-NO_2**, and **Z-NO·acetone** in the crystalline or solid state were carried out using SQUID magnetometers, and the resultant $\chi_M T-T$ plots are shown in Figure 9. The $\chi_M T$ values at ambient temperatures, 273 and 300 K, were collected in Table 2 (represented as $\chi_M T$(i)).

Z-CN exhibited a $\chi_M T$ of 3.3 cm^3 K mol^{-1} at 300 K, which was a typical value for HS Fe^{II} species.[2] $\chi_M T$ value did not change significantly upon cooling to 30 K. The abrupt decrease of $\chi_M T$ that emerged below 30 K is attributed to zero-field splitting[4] and/or intermolecular antiferromagnetic interaction.

dx.doi.org/10.1021/ic300030b | *Inorg. Chem.* 2012, 51, 5188−5198

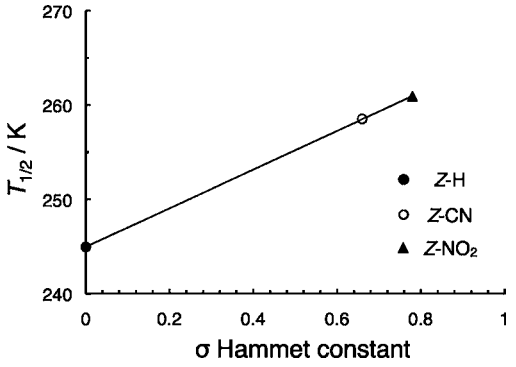

Figure 8. $T_{1/2}$ vs σ Hammet constant plots for the Fe^{II} SCO complexes.

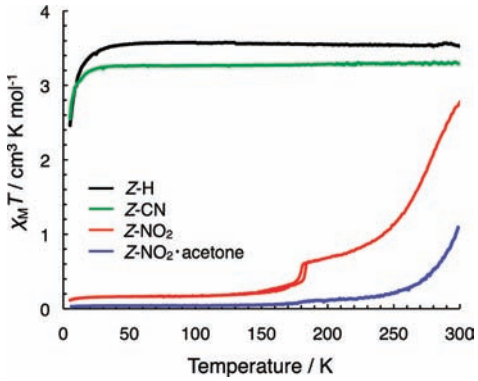

Figure 9. Temperature dependence of $\chi_M T$ for **Z-H**, **Z-CN**, **Z-NO_2**, and **Z-NO_2·acetone** in the microcrystalline state.

Thus, **Z-CN** occupied the HS state for the overall temperature range, just as **Z-H** with 3.6 cm^3 K mol^{-1} from 300 to 30 K. Therefore, the introduction of cyano groups did not influence the magnetic property remarkably in the microcrystalline state of the *Z*-form. On the other hand, **Z-NO_2** showed a smaller $\chi_M T$ of 2.8 cm^3 K mol^{-1} at 300 K and exhibited gradual thermal spin crossover, reaching a $\chi_M T$ of 0.20 cm^3 K mol^{-1} at 150 K. This result indicates that the introduction of nitro groups stabilized the LS state. In solution, the LS stabilization was observed in both **Z-CN** and **Z-NO_2**, whereas only **Z-NO_2** displayed the stabilization of the LS state in the solid state. The Hammett constant σ_p is 0.66 for a cyano group and 0.78 for a nitro group,[39] taking similar values with one another. This fact indicates that the substituent effect alone cannot sufficiently account for the contrastive magnetic behavior of **Z-CN** and **Z-NO_2** in the solid state. In **Z-NO_2**, a tiny thermal hysteresis around 180 K was found in the $\chi_M T$ vs T plot, suggesting that a kind of a phase transition occurred. DSC measurement supported the occurrence of a phase transition at this temperature range (Supporting Information, Figure S3). We could not clarify the detail of this phase transition at this stage, because we were not able to obtain the single crystal of unsolvated **Z-NO_2**. **Z-NO_2·acetone** exhibited a $\chi_M T$ of 1.1 cm^3 K mol^{-1} at 300 K and displayed thermal SCO around room temperatures to reach a $\chi_M T$ of 0.10 cm^3 K mol^{-1} at 170 K, taking the LS state below this temperature. The transition temperature $T_{1/2}$ of **Z-NO_2·acetone** (>300 K) was higher than that of **Z-NO_2** (ca. 270 K): Therefore, the LS state was further stabilized in **Z-NO_2·acetone**.

Magnetic susceptibility measurements were performed on the photoirradiated microcrystalline samples of **Z-H**, **Z-CN**, **Z-NO_2**, and **Z-NO_2·acetone**. $\chi_M T-T$ plots for the photoproducts are shown in Figure 10. All photoirradiated *Z*-form samples displayed incomplete thermal spin crossover. In **Z-CN**, a decrease in magnetization was observed upon *Z*-to-*E* photoisomerization over the entire temperature range: The photoirradiated sample exhibited a $\chi_M T$ value of 2.8 cm^3 K mol^{-1} at 300 K, and showed gradual thermal SCO, reaching a $\chi_M T$ value of 1.8 cm^3 K mol^{-1} at 100 K. These variations in the magnetic properties caused by visible light irradiation were similar to those of **Z-H**. The ratio of the $\chi_M T$ values varied no more than 20% under ambient temperatures (Table 2). In contrast, the $\chi_M T$ values of **Z-NO_2** increased after visible light irradiation. The irradiated sample yielded a thermal SCO and a constant $\chi_M T$ value of 2.0 cm^3 K mol^{-1} below 100 K. Variations in the ratio of $\chi_M T$ upon *Z*-to-*E* photoisomerization were as large as those observed for **Z-H** and **Z-CN** at 300 K, although the modulation was more prominent at 273 K (42%). Microcrystals of **Z-NO_2·acetone** presented a more profound photomagnetic effect. As with **Z-NO_2**, *Z*-to-*E* photoisomerization in **Z-NO_2·acetone** increased the values of $\chi_M T$. The photoirradiated sample then underwent thermal SCO with a constant $\chi_M T$ of 2.0 cm^3 K mol^{-1} below 100 K. The large variations in the ratio of $\chi_M T$ values were noteworthy: the variations reached 64% at 300 K and 87% at 273 K (Table 2). Thus, **Z-NO_2·acetone** displayed the largest variation in $\chi_M T$ among the four samples at ambient temperatures.

Single Crystal X-ray Crystallography. The crystal structures and crystallographic data for **Z-H** at 90 K, **Z-CN** and **Z-NO_2·acetone** at 113 K are shown in Figures 11a–c and Table 3. Fe–N bond distances and bite angles around the coordination sphere are good indicators of the spin state of Fe^{II} complexes.[2,40,41] Dipyrazolylpyridine ligand complexes yield an average Fe–N bond distance of 1.93–1.97 Å in LS complexes and 2.14–2.20 Å in HS complexes.[26,27,42–45] Also, the Σ parameter (deg), which is the summation of the

Table 2. $\chi_M T$ of the Fe^{II} Complexes before and after Photoirradiation at 300 and 273 K

	300 K				273 K			
	$\chi_M T$(i)[a] (cm^3 K mol^{-1})	$\chi_M T$(f)[b] (cm^3 K mol^{-1})	$\Delta\chi_M T$[c] (cm^3 K mol^{-1})	variation ratio[d] (%)	$\chi_M T$(i)[a] (cm^3 K mol^{-1})	$\chi_M T$(f)[b] (cm^3 K mol^{-1})	$\Delta\chi_M T$[c] (cm^3 K mol^{-1})	variation ratio[d] (%)
Z-H	3.6	3.1	0.5	14	3.6	3.0	0.6	17
Z-CN	3.3	2.8	0.5	15	3.3	2.7	0.6	18
Z-NO_2	2.8	3.2	0.4	12	1.8	3.1	1.3	42
Z-NO_2 ·acetone	1.1	3.1	2.0	64	0.4	3.0	2.6	87

[a] $\chi_M T$ value before photoirradiation. [b] $\chi_M T$ value at PSS. [c] $\Delta\chi_M T = |\chi_M T(f) - \chi_M T(i)|$. [d] $\Delta\chi_M T/\chi_M T(i)$ for **Z-H** and **Z-CN**, $\Delta\chi_M T/\chi_M T(f)$ for **Z-NO_2** and **Z-NO_2·acetone**.

dx.doi.org/10.1021/ic300030b | *Inorg. Chem.* 2012, 51, 5188–5198

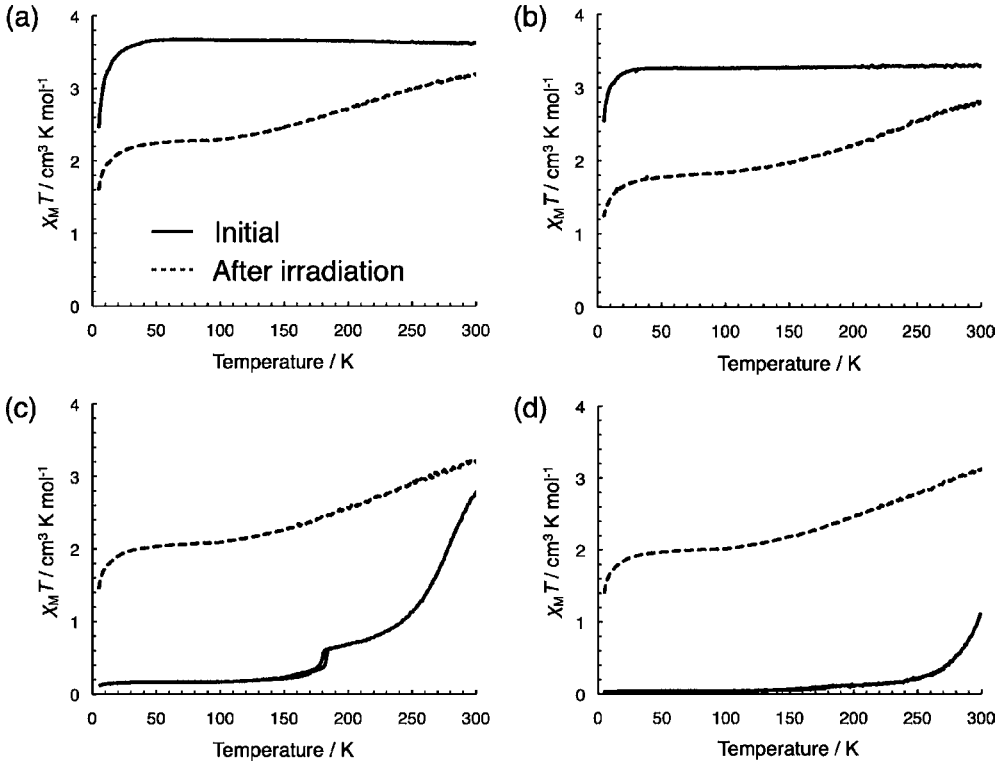

Figure 10. Temperature dependence of $\chi_M T$ for (a) ***Z*-H**, (b) ***Z*-CN**, (c) ***Z*-NO_2**, and (d) ***Z*-NO_2·acetone** before (solid lines) and after (broken lines) visible light (λ > 420 nm) irradiation for 115 h in ***Z*-H**, 94 h in ***Z*-CN**, and 72 h in ***Z*-NO_2** and ***Z*-NO_2·acetone**.

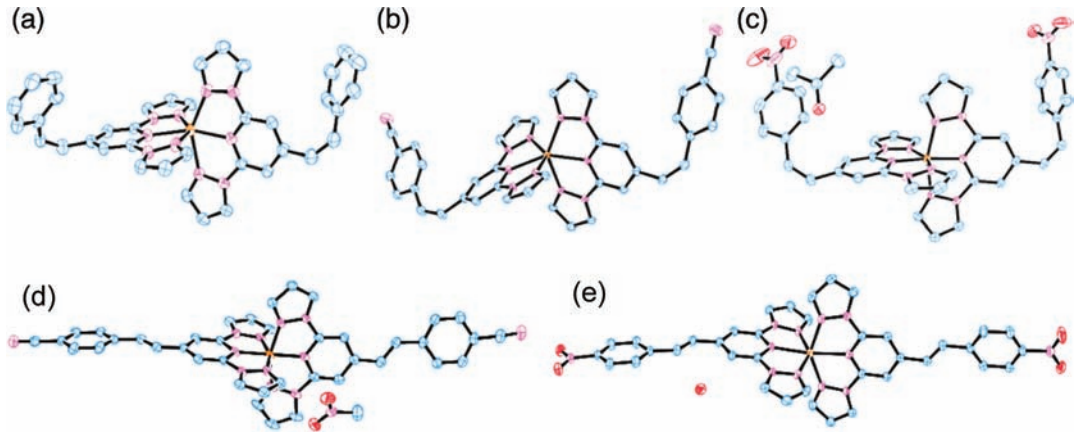

Figure 11. ORTEP diagrams showing 50% probability for (a) ***Z*-H**, (b) ***Z*-CN**, (c) ***Z*-NO_2·acetone**, (d) ***E*-CN·$MeNO_2$**, and (e) ***E*-NO_2·H_2O**. Diffraction data were collected at 113 K except for ***Z*-H** (90 K). Counter anions and hydrogen atoms are omitted for clarity.

deviations from 90° of the twelve bite angles around the central Fe^{II} ion,[46,47] can range from 85° to 96° in LS complexes and from 145° to 197° in HS complexes. In this study, the average Fe−N bond distance and Σ parameter were 2.170 Å and 172.4° for ***Z*-H** at 90 K, 2.171 Å and 183.1° for ***Z*-CN**, and 1.946 Å and 88.7° for ***Z*-NO_2·acetone** at 113 K, respectively. These results suggested that ***Z*-H** and ***Z*-CN** assumed a HS state and ***Z*-NO_2·acetone** assumed a LS state at those temperatures. These results were consistent with the magnetic susceptibility measurements (Figure 9). The *E*-forms were also subjected to single-crystal XRD analysis. The crystal structure of ***E*-H·2PC** had been reported in the previous communication,[26] whereas those of ***E*-CN·$MeNO_2$** and ***E*-NO_2·H_2O** were newly disclosed. (Figures 11d and 11e and Table 3).

The crystal packing structure notably revealed $\pi-\pi$ interactions between the pyrazole rings of ***Z*-H** and between the 4-cyanophenyl groups of ***Z*-CN** (Figures 12a and 12b). The $\pi-\pi$ interactions were expected to distort the coordination geometry away from ideal octahedral coordination at the Fe^{II} center (i.e., a large Σ parameter), which favored the HS state. Distortions in octahedral coordination spheres at Fe^{II} centers usually favor the HS state.[2,47] On the other hand, such $\pi-\pi$ interactions were absent from the ***Z*-NO_2·acetone** structure (Figure 12c), which appeared to assume an ideal octahedral coordination sphere that stabilized the LS state. Single crystals of solvent-free ***Z*-NO_2** have not yet been obtained, and the contribution of the acetone molecules to the ***Z*-NO_2·acetone** structure remains unknown. Because $T_{1/2}$ was higher in ***Z*-NO_2·acetone** than in the solvent-free ***Z*-NO_2**, the solvent

dx.doi.org/10.1021/ic300030b | *Inorg. Chem.* 2012, 51, 5188−5198

Table 3. Crystal Data for *Z*-H, *Z*-CN, *Z*-NO_2·acetone, *E*-CN·$MeNO_2$, and *E*-NO_2·H_2O

	Z-H	*Z*-CN	*Z*-NO_2·acetone
empirical formula	$C_{38}H_{30}N_{12}B_2F_8Fe$	$C_{20}H_{14}N_6BF_4Fe_{0.5}$	$C_{41}H_{34}N_{12}O_3B_2F_8Fe$
Fw	856.17	453.11	1004.27
crystal dimension	0.31 × 0.25 × 0.02 mm	0.16 × 0.10 × 0.03 mm	0.25 × 0.11 × 0.06 mm
crystal system	monoclinic	monoclinic	monoclinic
lattice parameters	*a* = 39.672(18) Å	*a* = 14.439(3) Å	*a* = 7.9954(13) Å
	b = 8.106(3) Å	*b* = 8.2491(17) Å	*b* = 36.339(6) Å
	c = 36.949(18) Å	*c* = 32.940(7) Å	c = 15.344(3) Å
	β = 140.303(7)°	*β* = 99.954(3)°	*β* = 98.374(2)°
	V = 7589(6) Å^3	*V* = 3864.6(14) Å^3	*V* = 4410.5(13) Å^3
space group	*C*2/*c*	*C*2/*c*	*P*21/*n*
Z value	8	8	4
λ	0.7107 Å	0.7107 Å	0.7107 Å
T	90 K	113 K	113 K
μ(Mo K*α*)	0.481 mm^{-1}	0.479 mm^{-1}	0.436 mm^{-1}
D(calc)	1.498 g/cm^3	1.558 g/cm^3	1.512 g/cm^3
R_1	0.0927	0.0596	0.0815
WR_2	0.2659	0.1383	0.2158
GOF	1.098	1.164	1.096

	E-CN·$MeNO_2$	*E*-NO_2·H_2O
empirical formula	$C_{41}H_{31}N_{13}O_2B_2F_8Fe$	$C_{38}H_{30}N_{12}O_5B_2F_8Fe$
Fw	967.26	962.19
crystal dimension	0.17 × 0.16 × 0.06 mm	0.10 × 0.10 × 0.07 mm
crystal system	triclinic	triclinic
lattice parameters	*a* = 11.9220(17) Å	*a* = 10.832(6) Å
	b = 12.8890(19) Å	*b* = 13.326(7) Å
	c = 14.539(2) Å	*c* = 16.010(9) Å
	α = 87.253(6)°	*α* = 107.925(6)°
	β = 80.397(5)°	*β* = 101.946(5)°
	γ = 70.184(4)°	*γ* = 104.959(6)°
	V = 2072.3(5) Å^3	*V* = 2018.6(19) Å^3
space group	$P\bar{1}$	$P\bar{1}$
Z value	2	2
λ	0.7107 Å	0.7107 Å
T	113 K	113 K
μ(Mo K*α*)	0.456 mm^{-1}	0.472 mm^{-1}
D(calc)	1.550 g/cm^3	1.583 g/cm^3
R_1	0.0654	0.0608
WR_2	0.1839	0.1646
GOF	1.048	1.094

molecules may further stabilize the LS state, for example, by filling up the voids in the crystal lattice to support the ***Z*-NO$_2$·acetone** crystal structure without the need for *π*−*π* interactions. Intermolecular interactions and guest solvent inclusion are expected to dominate the magnetic properties of complexes rather than the electronic substituent effects. We note that crystal packing and crystal solvents significantly affect the magnetic properties of [Fe^{II}(2,6-di(1*H*-pyrazol-1-yl)-4-pyridine)$_2$] complexes.[44,45,47]

Because all photoproducts were amorphous, quantitative analysis of the bond lengths and intermolecular interactions of the photogenerated *E*-forms is impossible. Hereafter, limited discussion is described. The $\chi_M T-T$ plots of the photo-irradiated ***Z*-NO$_2$** and ***Z*-NO$_2$·acetone** resemble one another (Figure 10). This experimental fact indicates that the two photogenerated materials are in the same status: In fact, the FT-IR spectrum of photoirradiated ***Z*-NO$_2$·acetone** does not contain any peaks for acetone molecules (Supporting Information, Figure S4). Therefore, the acetone molecules as the crystal solvent are released in the course of *Z*-to-*E* photoisomerization. Greater magnetization in ***Z*-NO$_2$** and ***Z*-NO$_2$·acetone** upon *Z*-to-*E* photoisomerization would result from the emergence of new intermolecular interactions in the amorphous solid to stabilize the HS state. In other words, changes in intermolecular interactions, often expressed as chemical pressure and anisotropy,[1,2] would accompany the *Z*-to-*E* photoisomerization, to influence the spin state. This contribution would work more dominantly than the intensification of the ligand field induced by the intramolecular *Z*-to-*E* photoisomerization, which stabilizes the LS state. The steep decline of the $\chi_M T$ values in ***Z*-H** and ***Z*-CN** may be due to the cancellation of strong intermolecular *π*−*π* interactions, although strengthening of the ligand field upon *Z*-to-*E* photoisomerization could not be excluded.

Variable-temperature magnetic susceptibility measurements were also carried out for the synthesized ***E*-CN** and ***E*-NO$_2$**. Microcrystalline samples of the two complexes displayed gradual and incomplete thermal spin crossover to reach a $\chi_M T$ value of 1.0 cm^3 K mol^{-1} below 90 K (Supporting Information, Figure S5). The magnetic properties of the

dx.doi.org/10.1021/ic300030b | *Inorg. Chem.* 2012, 51, 5188−5198

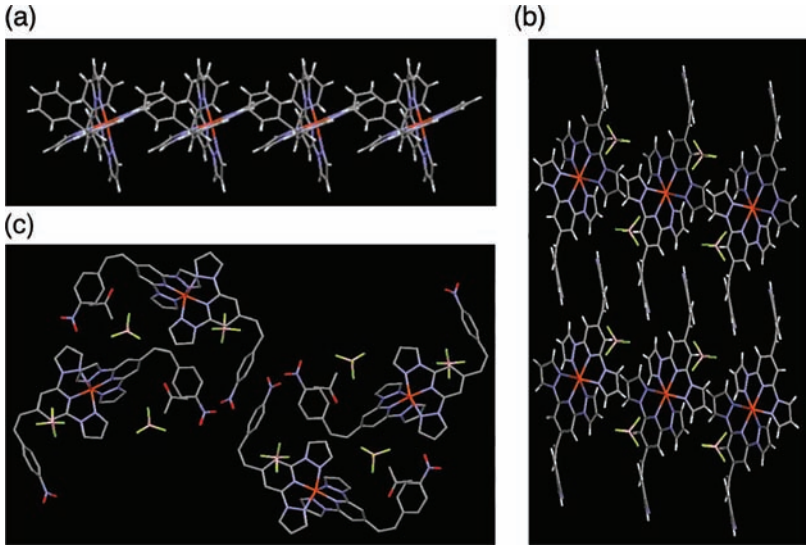

Figure 12. Crystal packings of (a) **Z-H** along *c* axis, (b) **Z-CN** along *a* axis, and (c) **Z-NO_2·acetone** along *a* axis. Counter anions (a) and hydrogen atoms (c) are omitted for clarity.

synthesized *E*-form complexes were not completely consistent with those of the photogenerated *E*-forms, which might stem from differences in intermolecular interactions, presence or absence of crystal solvents, and crystal lattice effects.[48]

■ CONCLUSIONS

We synthesized analogues of an Fe^{II} complex, $[Fe^{II}(2,6\text{-di}(1H\text{-pyrazol-1-yl})\text{-4-styrylpyridine})_2](BF_4)_2$, which displayed LD-LISC behavior at ambient temperatures. Cyano and nitro groups were introduced at the tips of the stilbene moieties to enhance modulation of the photomagnetism. These substituents did not affect the one-way *Z*-to-*E* photoisomerization in solution or microcrystalline solid states. In the solution phase, cyano and nitro groups stabilized the LS state in proportion to the groups' electron-withdrawing strength. In contrast, the substituents affected the photomagnetic properties in the microcrystalline and solid states in such a way that was not fully attributable to the electronic effects. The single crystal X-ray structures of the *Z*-forms were associated with the magnetism of the structures. **Z-H** and **Z-CN**, in the HS state at any temperature, included intermolecular $\pi-\pi$ interactions that distorted the octahedral coordination environment at the Fe^{II} center, thereby stabilizing the HS state. On the other hand, **Z-NO_2·acetone** preferred the LS state. In this complex, $\pi-\pi$ interactions were absent, and distortion of the Fe^{II} coordination sphere was negligible. The LS state of this structure was thereby stabilized. **Z-NO_2** partially destabilized the LS state compared to **Z-NO_2·acetone**. This result indicated that the solvent molecules also stabilized the LS state. *Z*-to-*E* photoisomerization suppressed magnetization in the **Z-H** and **Z-CN** structures and increased $\chi_M T$ in **Z-NO_2** and **Z-NO_2·acetone**. **NO_2·acetone** displayed the most profound LD-LISC effects at ambient temperatures.

■ EXPERIMENTAL SECTION

Materials. Solvents and reagents were used as received unless otherwise noted. (2,6-di(1*H*-pyrazol-1-yl)pyridin-4-yl)-isonicotinaldehyde[49,50] and tris(2-(methoxymethoxy)phenyl)-phosphine[51,52] were synthesized according to the literature procedures. The syntheses of **Z-H** and ***E*-H** were reported in our previous paper.[26] 4-Cyanobenzyl bromide and (4-cyanobenzyl)phosphonic acid diethyl ester were obtained from TCI Ltd. 4-Nitrobenzyl bromide and iron(II) tetrafluoroborate hexahydrate were received from Aldrich Ltd. *n*-Buthyllithium in hexane and manganese dioxide were obtained from Kanto Ltd. Silica gel 60 (0.040−0.064 mm) for a flash silica column chromatography was purchased from MERCH Ltd. Dichloromethane used as a solvent for reactions was distilled from calcium hydride under a nitrogen atmosphere. Tetrahydrofuran (THF) used as a solvent for reactions was distilled from sodium and benzophenone under a nitrogen atmosphere. Spectroscopy grade acetonitrile was obtained from Kanto Chemical Ltd. Potassium bromide (Wako Ltd.) for FT-IR spectroscopy was stored in a drybox and used as it was. Common solvents and anhydrous solvents used for syntheses and measurements were obtained from Kanto Chemical Ltd.

Synthesis of 4-Cyanobenzyltris(2-(methoxymethoxy)-phenyl)phosphonium Bromide. Tris(2-(methoxymethoxy)-phenyl)phosphine (1.00 g, 2.26 mmol), 4-cyanobenzyl bromide (576 mg, 2.94 mmol), and sodium hydrogen carbonate (134 mg, 1.60 mmol) were dissolved in 10 mL of acetonitrile and heated to 80 °C for 10 min. After evaporation of the solvent, the residue was extracted with dichloromethane (50 mL) and filtered. The filtrate was concentrated, and ethyl acetate (30 mL) was added to give rise to pale white precipitate, which was filtered and washed by ethyl acetate. The titled compound was obtained as a white powder. Yield: 1.34 g (2.10 mmol, 93%). ^{1}H NMR (acetone-d_6, 295 K): δ 7.88 (dd, J = 15.1, 7.9 Hz, 3H, Ph), 7.83−7.79 (m, 3H, Ph), 7.58 (d, J = 8.0 Hz, 2H, Bz) 7.50 (dd, J = 8.3, 2.0 Hz, 2H, Bz), 7.39−7.32 (m, 6H, Ph), 5.30 (d, J = 16.1 Hz, 2H, CH_2), 5.21 (s, 6H, CH_2), 3.10 (s, 9H, CH_3). Analytical data. Found: C, 60.00; H, 5.38; N, 2.13%. Calcd for $C_{32}H_{33}O_6NBrP$: C, 60.20; H, 5.21; N, 2.19%.

Synthesis of (*Z*)-2,6-di(1*H*-pyrazol-1-yl)-4-(4-cyanostyryl)-pyridine. Under a nitrogen atmosphere, 4-cyanobenzyltris(2-(methoxymethoxy)phenyl)phosphonium bromide (670 mg, 1.05 mmol) was suspended in 50 mL of dry THF. This suspension was then stirred, and *n*-buthyllithium (1.65 M in hexane, 0.70 mL, 1.1 mmol) was added dropwise at 0 °C. The reaction mixture was warmed to room temperature, and was turned from white suspension to orange suspension after 1 h, and then, 2,6-di(1*H*-pyrazol-1-yl)-isonicotinaldehyde (250 mg, 1.05 mmol) in 30 mL of dry THF was added dropwise at −78 °C. The reaction mixture was kept stirred at −78 °C for 2 h. After warming to room temperature, THF was removed under vacuum. The residue was suspended in 20 mL of chloroform, and filtered through *Celite* to remove lithium bromide. The filtrate, which contained *Z*- and *E*-isomers, was chromatographed on alumina with chloroform−hexane (1:1). The titled compound was obtained as a white solid. Yield: 175 mg (0.52 mmol, 50%). ^{1}H NMR

dx.doi.org/10.1021/ic300030b | *Inorg. Chem.* 2012, 51, 5188−5198

($CDCl_3$, 295 K): δ 8.54 (dd, J = 2.6, 0.5 Hz, 2H, Pz), 7.71 (d, J = 1.0 Hz, 2H, Pz), 7.66 (s, 2H, Py), 7.54 (dd, J = 8.4, 1.7 Hz, 2H, Ph), 7.37 (d, J = 8.2 Hz, 2H, Ph), 6.85 (d, J = 12.3 Hz, 1H, CH═C*H*), 6.77 (d, J = 12.3 Hz, 1H, CH═C*H*), 6.49 (dd, J = 2.6, 1.7 Hz, 2H, Pz). ESI-TOF mass (positive, acetonitrile): m/z = 339.10 $[M + H]^+$, calcd for $C_{20}H_{15}N_6$, 339.13. Analytical data. Found: C, 70.91; H, 4.41; N, 24.55%. Calcd for $C_{20}H_{14}N_6$: C, 70.99; H, 4.17; N, 24.84%.

Synthesis of *Z*-CN. Under a nitrogen atmosphere, (*Z*)-2,6-di(1*H*-pyrazol-1-yl)-4-(4-cyanostyryl)pyridine (80 mg, 0.24 mmol) was dissolved in 10 mL of dry acetone. $Fe(BF_4)_2{\cdot}6H_2O$ (39 mg, 0.12 mmol) dissolved in 2 mL of dry acetone was added to the former stirred solution at room temperature. The reaction mixture immediately turned from colorless solution to red solution. After stirring for 30 min, most of the solution was evaporated under a stream of nitrogen at room temperature. The residue was recrystallized from acetone/diethyl ether. The precipitate was filtered and washed by diethyl ether. After being dried under vacuum at 100 °C, **Z-CN** was obtained as orange powder. Yield: 96 mg (0.11 mmol, 92%). ESI-TOF mass (positive, acetonitrile): m/z = 366.18 $[M]^{2+}$, calcd for $C_{40}H_{28}N_{12}Fe$, 366.10. Analytical data. Found: C, 52.85; H, 3.34; N, 18.36%. Calcd for $C_{40}H_{28}N_{12}B_2F_8Fe$: C, 53.02; H, 3.11; N, 18.55%.

Synthesis of (*E*)-2,6-di(1*H*-pyrazol-1-yl)-4-(4-cyanostyryl)-pyridine. Under a nitrogen atmosphere, (4-cyanobenzyl)phosphonic acid diethyl ester (267 mg, 1.05 mmol) was suspended in 20 mL of dry THF. To the former stirred solution, *n*-buthyllithium (1.63 M in hexane, 0.70 mL, 1.1 mmol) was added dropwise at 0 °C. The reaction mixture was warmed to room temperature, and turned from a white suspension to a yellow suspension after 1 h. Then, 2,6-di(1*H*-pyrazol-1-yl)isonicotinaldehyde (252 mg, 1.05 mmol) in 20 mL of dry THF was added dropwise at room temperature, and the reaction mixture turned to a green solution. After stirring for 2 h, THF was removed under vacuum. The residue was suspended in 30 mL of chloroform, and filtered through *Celite* to remove lithium bromide. The filtrate, which contained both *Z*- and *E*-isomers, was chromatographed on alumina with chloroform−hexane (1:1). The title compound was collected, and recrystallized from dichloromethane/hexane, to afford the title compound as a white solid. Yield: 247 mg (0.73 mmol, 69%). ^{1}H NMR (acetone-d_6, 295 K): δ 8.86 (dd, J = 2.6, 0.6 Hz, 2H, Pz), 8.10 (s, 2H, Py), 8.03 (d, J = 8.3 Hz, 2H, Ph), 7.88 (d, J = 17.6 Hz, 1H, CH═C*H*), 7.87 (d, J = 8.3 Hz, 2H, Ph), 7.84 (dd, J = 1.6, 0.5 Hz, 2H, Pz), 7.70 (d, J = 16.4 Hz, 1H, CH═C*H*), 6.59 (dd, J = 2.6, 1.6 Hz, 2H, Pz). MALDI-TOF mass: m/z = 339.12 $[M + H]^+$, calcd for $C_{20}H_{15}N_6$, 339.13. Analytical data. Found: C, 69.19; H, 4.39; N, 24.11%. Calcd for $C_{20}H_{14}N_6{\cdot}0.5H_2O$: C, 69.15; H, 4.35; N, 24.19%.

Synthesis of *E*-CN. Under a nitrogen atmosphere, (*E*)-2,6-di(1*H*-pyrazol-1-yl)-4-(4-nitrostyryl)pyridine (100 mg, 0.29 mmol) was dissolved in 15 mL of dry acetone. To this stirred solution was added $Fe(BF_4)_2{\cdot}6H_2O$ (48 mg, 0.14 mmol) dissolved in 2 mL of dry acetone at room temperature. The reaction mixture immediately turned from a colorless solution to a red suspension. After stirring for 30 min, the precipitate was filtered and washed by 2 mL of ice-cold acetone and diethyl ether. After recrystallization from nitromethane/dietyl ether and under vacuum at 100 °C, ***E*-CN** was obtained as orange solid. Yield: 118 mg (0.13 mmol, 92%). ESI-TOF mass (positive, acetonitrile): m/z = 366.00 $[M]^{2+}$, calcd for $C_{40}H_{28}N_{12}Fe$, 366.10. Analytical data. Found: C, 50.55; H, 3.39; N, 17.48%. Calcd for $C_{40}H_{28}N_{12}B_2F_8Fe{\cdot}2.5H_2O$: C, 50.51; H, 3.50; N, 17.67%.

Synthesis of 4-Nitrobenzyltris(2-(methoxymethoxy)phenyl)-phosphonium Bromide. Tris(2-(methoxymethoxy)phenyl)-phosphine (5.97 g, 13.5 mmol), 4-nitrobenzyl bromide (3.81 g, 17.6 mmol), and sodium hydrogen carbonate (0.81 g, 9.6 mmol) were dissolved in 60 mL of acetonitrile and heated to 80 °C for 10 min. After evaporation of the solvent, the residue was extracted with dichloromethane (100 mL), and insoluble materials were filtered off. The filtrate was concentrated, and ethyl acetate (60 mL) was added to form a pale yellow precipitate, which was collected and washed by ethyl acetate. The title compound was obtained as pale yellow powder. Yield: 8.33 g (12.7 mmol, 94%). ^{1}H NMR (acetone-d_6, 295 K): δ 8.02 (d, J = 8.1 Hz, 2H, Bz), 7.86 (dd, J = 15.1, 7.8 Hz, 3H, Ph), 7.82−7.78 (m, 3H, Ph), 7.56 (dd, J = 8.5, 2.0 Hz, 2H, Bz), 7.38−7.31 (m, 6H, Ph), 5.34 (d, J = 16.1 Hz, 2H, CH_2), 5.20 (s, 6H, CH_2), 3.10 (s, 9H, CH_3). Analytical data. Found: C, 55.79; H, 5.05; N, 2.13%. Calcd for $C_{31}H_{33}O_8NBrP{\cdot}0.5H_2O$: C, 55.78; H, 5.13; N, 2.10%.

Synthesis of (*X*)-2,6-di(1*H*-pyrazol-1-yl)-4-(4-nitrostyryl)-pyridine (*X* = *Z*, *E*). Under a nitrogen atmosphere, 4-nitrobenzyltris-(2-(methoxymethoxy)phenyl)phosphonium bromide·0.5H_2O (1.38 g, 2.06 mmol) was suspended in 90 mL of dry THF. To the former stirred solution, *n*-buthyllithium (1.6 M in hexane, 1.3 mL, 2.1 mmol) was added dropwise at 0 °C. The reaction mixture was warmed to room temperature, and turned from a white suspension to a dark-red suspension after 1 h, and then, 2,6-di(1*H*-pyrazol-1-yl)-isonicotinaldehyde (500 mg, 2.09 mmol) in 90 mL of dry THF was added dropwise at −78 °C. The reaction mixture was kept stirred at −78 °C for 3 h, and at room temperature for 12 h. Afterwards, THF was removed under vacuum. The residue was suspended in 40 mL of chloroform, and filtered through *Celite* to remove lithium bromide. The filtrate, which contained both *Z*- and *E*-isomers, was chromatographed on alumina with chloroform−hexane (3:1). *Z*- and *E*- isomers were collected separatedly. The pure products were obtained by recrystallization from dichloromethane/hexane.

(Z)-2,6-Di(1H-pyrazol-1-yl)-4-(4-nitrostyryl)pyridine. Obtained as white solid. Yield: 181 mg (0.51 mmol, 25%). ^{1}H NMR ($CDCl_3$, 295 K): δ 8.54 (dd, J = 2.7, 0.7 Hz, 2H, Pz), 8.11 (d, J = 8.8 Hz, 2H, Ph), 7.70 (dd, J = 1.4, 0.5 Hz, 2H, Pz), 7.68 (s, 2H, Py), 7.43 (d, J = 8.5 Hz, 2H, Ph), 6.90 (d, J = 12.4 Hz, 1H, CH═C*H*), 6.82 (d, J = 12.4 Hz, 1H, CH═C*H*), 6.48 (dd, J = 2.4, 1.7 Hz, 2H, Pz). ESI-TOF mass (positive, acetonitrile): m/z = 381.1047 $[M + Na]^+$, calcd for $C_{19}H_{14}O_2N_6Na$, 381.1076. Analytical data. Found: C, 63.50; H, 4.11; N, 23.31%. Calcd for $C_{19}H_{14}O_2N_6$: C, 63.68; H, 3.94; N, 23.45%.

(E)-2,6-Di(1H-pyrazol-1-yl)-4-(4-nitrostyryl)pyridine. Obtained as yellow microcrystals. Yield: 210 mg (0.59 mmol, 29%). ^{1}H NMR (CD_2Cl_2, 295 K): δ 8.60 (dd, J = 2.7, 0.7 Hz, 2H, Pz), 8.28 (d, J = 8.8 Hz, 2H, Ph), 8.01 (s, 2H, Py), 7.81 (d, J = 1.0 Hz, 2H, Pz), 7.71 (d, J = 8.8 Hz, 2H, Ph), 7.56 (d, J = 17.0 Hz, 1H, CH═C*H*), 7.29 (d, J = 16.4 Hz, 1H, CH═C*H*), 6.53 (dd, J = 2.7, 1.7 Hz, 2H, Pz). ESI-TOF mass (positive, acetonitrile): m/z = 381.1073 $[M + Na]^+$, calcd for $C_{19}H_{14}O_2N_6Na$, 381.1076. Analytical data. Found: C, 63.66; H, 4.09; N, 23.36%. Calcd for $C_{19}H_{14}O_2N_6$: C, 63.68; H, 3.94; N, 23.45%.

Synthesis of *Z*-NO_2. Under a nitrogen atmosphere, (*Z*)-2,6-di(1*H*-pyrazol-1-yl)-4-(4-nitrostyryl)pyridine (52 mg, 0.15 mmol) was dissolved in 10 mL of dry acetone. $Fe(BF_4)_2{\cdot}6H_2O$ (24 mg, 0.071 mmol) dissolved in 2 mL of dry acetone was added to this solution at room temperature. The reaction mixture immediately turned from colorless to red. After stirring for 30 min, most of the solvent was evaporated under a stream of nitrogen at room temperature. The residue was recrystallized from acetone/diethyl ether. The precipitate was filtered and washed by diethyl ether. After drying under vacuum at 100 °C, **Z-NO_2** was obtained as orange microcrystals. Yield: 55 mg (0.058 mmol, 82%). ESI-TOF mass (positive, acetonitrile): m/z = 386.10 $[M]^{2+}$, calcd for $C_{38}H_{28}O_4N_{12}Fe$, 386.09. Analytical data. Found: C, 48.06; H, 3.19; N, 17.64%. Calcd for $C_{38}H_{28}O_4N_{12}B_2F_8Fe$: C, 48.24; H, 2.98; N, 17.76%.

Synthesis of *E*-NO_2. Under a nitrogen atmosphere, (*E*)-2,6-di(1*H*-pyrazol-1-yl)-4-(4-nitrostyryl)pyridine (100 mg, 0.28 mmol) was dissolved in 12 mL of dry acetone. $Fe(BF_4)_2{\cdot}6H_2O$ (46 mg, 0.14 mmol) dissolved in 5 mL of dry acetone was added to the former stirred solution at room temperature. The reaction mixture immediately turned from colorless solution to dark-red suspension. After stirring for 30 min, about 2/3 of the volume was slowly evaporated under a stream of nitrogen at room temperature, forming a red precipitate. The precipitate was filtered and washed with 2 mL of acetone. After recrystallization from nitromethane/dietyl ether and under vacuum at 100 °C, ***E*-NO_2** was obtained as red microcrystals. Yield: 112 mg (0.12 mmol, 86%). ESI-TOF mass (positive, acetonitrile): m/z = 386.11 $[M]^{2+}$, calcd for $C_{38}H_{28}O_4N_{12}Fe$, 386.09. Analytical data. Found: C, 46.09; H, 3.32; N, 16.92%. Calcd for $C_{38}H_{28}O_4N_{12}B_2F_8Fe{\cdot}2.5H_2O$: C, 46.05; H, 3.36; N, 16.96%.

Photoirradiation Experiments. For solution samples and KBr-pelletized samples, the light source for solution samples was supplied by a high-pressure mercury lamp (USH-500D, Ushio), and the bright

dx.doi.org/10.1021/ic300030b | *Inorg. Chem.* 2012, 51, 5188−5198

lines were separated by a monochromator (Jasco CT-10T) to extract 436 nm light with an intensity of 2.5 mW/cm^2. For the solid samples, light from a high-pressure mercury lamp was allowed to get through a UV cut filter to reduce $\lambda < 420$ nm light. The intensity of the light of $\lambda > 420$ nm was about 200 mW/cm^2. Photoirradiation was conducted at 295 K.

Preparation of Microcrystalline Samples. Solvent-free microcrystals of **Z-H** and **Z-CN** were obtained by recrystallization from acetone/diethyl ether. On the other hand, recrystallization in various solvents did not provide us solvent-free microcrystals of **Z-NO$_2$**; instead, those including solvent molecules **Z-NO$_2$·acetone** were obtained by recrystallization from acetone/diethyl ether. Elemental analysis and thermogravimetric analysis (TGA) supported that the microcrystals of **Z-NO$_2$·acetone** contained one acetone molecule per one **Z-NO$_2$** (Supporting Information, Figure S6). **Z-H**, **Z-CN**, and **Z-NO$_2$·acetone** were investigated by means of single-crystal XRD (Figure 11 and Table 3). Solvent-free **Z-NO$_2$** was eventually obtained by vacuuming **Z-NO$_2$·acetone** at 373 K. Microcrystals of **E-CN** and **E-NO$_2$** were fabricated by recrystallization from nitromethane/dietyl ether, the compositions of which proved to be **E-CN·MeNO$_2$** and **E-NO$_2$·H$_2$O** by means of single-crystal XRD (Figure 11 and Table 3).

Magnetic Susceptibilities in Solution. Magnetic susceptibilities were measured by a paramagnetic shift of a reference TMS signal in ^{1}H NMR spectra (the Evans method)[38] using acetone-d_6 containing 1 vol % TMS as a solvent with a Bruker 500 MHz spectrometer equipped with a variable-temperature unit. A 5 mmϕ clear fused quartz tube (528-PP-7QZ, Wilmad Labglass, Buena, NJ) and a 2 mmϕ stem coaxial insert (528-PP-7QZ, Wilmad Labglass, Buena, NJ) were utilized as a cell. A concentration of Fe^{II} complexes was fabricated to be 1.00×10^{-3} M, and 1.0 equivalent of corresponding ligand was added to prevent ligand dissociations. The molar magnetic susceptibilities were corrected with the diamagnetism of the complexes and ligands, which were calculated from Pascal's constants. Diamagnetic susceptibilities were estimated to be -441×10^{-6} cm^3 mol^{-1} for **Z-H**, -464×10^{-6} cm^3 mol^{-1} for **Z-CN**, and -466×10^{-6} cm^3 mol^{-1} for **Z-NO$_2$** with one equivalent of their corresponding ligand. Changes in density of the solutions were corrected according to the literature.[53]

The fractions of the HS and LS species, γ_{HS} and γ_{LS}, at each temperature were calculated from the experimental data under an assumption of $\chi_M T$ being 3.75 cm^3 K mol^{-1} and 0 cm^3 K mol^{-1} for the HS and LS states, respectively. The equilibrium constant was defined as eq 1

$$K = \gamma_{HS}/\gamma_{LS} \quad (1)$$

The calculated ln K was ploted versus $1/T$, so as to find a linear relationship in each complex (Figure 6). Provided van't Hoff eq 2 is valid, thermodynamic parameters can be extracted from the slope and intercept of the ln K vs $1/T$ plot:

$$\ln K = -\Delta H/RT + \Delta S/R \quad (2)$$

where ΔH and ΔS are activation enthalpy and entropy, respectively. Then $T_{1/2}$ that gives $K = 1$ can be calculated as follows:

$$T_{1/2} = \Delta H/\Delta S \quad (3)$$

SQUID Measurements. Magnetic susceptibilities in the solid state were measured with an applied magnetic field of 10000 Oe, in a temperature range of 5−300 K, and at a rate of 1 K min^{-1} (sweep mode) with a Quantum Design MPMS SQUID magnetometer. Aluminum foils (Nippaku, Inc.) were used as sample containers for the measurements. The magnetic contribution of aluminum foils was always subtracted. Typical weights of aluminum foils and samples were 12 mg and 1.5 mg, respectively, and the typical heights of the samples were 4 mm. The molar magnetic susceptibilities were corrected with the diamagnetism of the complexes, which were calculated from Pascal's constants. Diamagnetic susceptibilities were estimated to be -324×10^{-6} cm^3 mol^{-1} for **Z-H**, -340×10^{-6} cm^3 mol^{-1} for **Z-CN**, -341×10^{-6} cm^3 mol^{-1} for **Z-NO$_2$**, and -375×10^{-6} cm^3 mol^{-1} for **Z-NO$_2$·acetone**.

Single-Crystal X-ray Structure Analysis. Diffraction data were collected with a Rigaku AFC10 diffractometer with a Rigaku Saturn 70CCD system equipped with a rotating-anode X-ray generator. Single crystals suitable for this analysis were mounted on a loop fiber with liquid paraffin. Graphite-monochromated Mo K_α radiation (λ = 0.71073 Å) was utilized. The diffraction data were integrated and compensated with numerical correction with the Crystal Clear 1.3.6 program. The structure was solved with SIR-92[54] and the whole structure was refined using SHELXL-97[55] by the full-matrix least-squares techniques on F^2. All calculations were performed using WinGX-1.70.01[56] software package. All non-hydrogen atoms were refined anisotropically. Hydrogen atoms of Fe^{II} complexes were located in the idealized positions and were refined using a riding model with fixed thermal parameters.

Other Measurements and Apparatus. ^{1}H NMR spectra were recorded with a JEOL AL-400 (400 MHz) or a Bruker DRX-500 (500 MHz) spectrometer. ESI-TOF-MS spectra were recorded with a Micromass LCT, a time-of-flight mass spectrometer. MALDI-TOF-MS spectra were recorded with a Shimadzu AXIMA-CER. UV−vis spectra in solutions were recorded with a JASCO V-570 spectrometer at 295 K. Quartz cells (optical path: 1 cm) were used for the measurement. FT-IR spectra were recorded with a JASCO FT/IT-620 V spectrometer. All spectra were measured as KBr pellets. A blank spectrum was measured by the use of clean KBr pellets as a reference sample before the measurement of each compound.

■ ASSOCIATED CONTENT

Ⓢ Supporting Information

FT-IR spectra of **Z-CN** and **Z-NO$_2$** in KBr pellets before and after irradiation with visible light (Figure S1), PXRD pattern for **Z-NO$_2$** before and after visible light irradiation (Figure S2), DSC of **Z-NO$_2$** (Figure S3), FT-IR spectrum of **Z-NO$_2$·acetone** after visible light irradiation (Figure S4), temperature dependence of $\chi_M T$ for **E-CN** and **E-NO$_2$** (Figure S5), TGA chart of **Z-NO$_2$·acetone** (Figure S6). This material is available free of charge via the Internet at http://pubs.acs.org.

■ AUTHOR INFORMATION

Corresponding Author

*E-mail: nisihara@chem.s.u-tokyo.ac.jp.

Notes

The authors declare no competing financial interest.

■ ACKNOWLEDGMENTS

The authors acknowledge Grants-in-Aid from MEXT of Japan (Nos. 20245013 and 21108002, area 2107, Coordination Programming) and the Global COE Program for Chemistry Innovation for financial support.

■ REFERENCES

(1) Gütlich, P.; Hauser, A.; Spiering, H. *Angew. Chem., Int. Ed. Engl.* **1994**, *33*, 2024−2054.
(2) In *Spin crossover in Transition Metal Compounds I-III*; Gütlich, P., Goodwin, H. A., Eds.; *Topics in Current Chemistry*; Springer-Verlag: Berlin, Germany, 2004; Vols. 233−235.
(3) Real, J. A.; Gaspara, A. B.; Muñoz, M. C. *Dalton Trans.* **2005**, 2062−2079.
(4) Létard, J.-F. *J. Mater. Chem.* **2006**, *16*, 2550−2559.
(5) Decurtins, S.; Gütlich, P.; Köhler, C. P.; Spiering, H.; Hauser, A. *Chem. Phys. Lett.* **1984**, *105*, 1−4.
(6) Létard, J.-F.; Capes, L.; Chastanet, G.; Moliner, N.; Létard, S.; Real, J. A.; Kahn, O. *Chem. Phys. Lett.* **1999**, *313*, 115−120.
(7) Marcen, S.; Lecren, L.; Capes, L.; Goodwin, H. A.; Létard, J.-F. *Chem. Phys. Lett.* **2002**, *358*, 87−95.

(8) Létard, J.-F.; Guionneau, P.; Nguyen, O.; Costa, J. S.; Marcén, S.; Chastanet, G.; Marchivie, M.; Goux-Capes, L. *Chem.—Eur. J.* **2005**, *11*, 4582−4589.
(9) Niel, V.; Gaspar, A. B.; Muñoz, M. C.; Abarca, B.; Ballesteros, R.; Real, J. A.; Zhang, L. *Inorg. Chem.* **2003**, *42*, 4782−4788.
(10) Hayami, S.; Kawajiri, R.; Juhasz, G.; Kawahara, T.; Hashiguchi, K.; Sato, O.; Inoue, K.; Maeda, Y. *Bull. Chem. Soc. Jpn.* **2003**, *76*, 1207−1213.
(11) Neville, S. M.; Leita, B. A.; Halder, G. J.; Kepert, C. J.; Moubaraki, B.; Létard, J.-F.; Murray, K. S. *Chem.—Eur. J.* **2008**, *14*, 10123−10133.
(12) Zhang, L.; Xu, G.-C.; Xu, H.-B.; Mereacre, V.; Wang, Z.-M.; Powell, A. K.; Gao, S. *Dalton Trans.* **2010**, *39*, 4856−4868.
(13) Yamada, M.; Fukumoto, E.; Ooidemizu, M.; Bréfuel, N.; Matsumoto, N.; Iijima, S.; Kojima, M.; Re, N.; Dahan, F.; Tuchagues, J.-P. *Inorg. Chem.* **2005**, *44*, 6967−6974.
(14) Sunatsuki, Y.; Ohta, H.; Kojima, M.; Ikuta, Y.; Goto, Y.; Matsumoto, N.; Iijima, S.; Akashi, H.; Kaizaki, S.; Dahan, F.; Tuchagues, J.-P. *Inorg. Chem.* **2004**, *43*, 4154−4171.
(15) Yamada, M.; Ooidemizu, M.; Ikuta, Y.; Osa, S.; Matsumoto, N.; Iijima, S.; Kojima, M.; Dahan, F.; Tuchagues, J.-P. *Inorg. Chem.* **2003**, *42*, 8406−8416.
(16) Ikuta, Y.; Ooidemizu, M.; Yamahata, Y.; Yamada, M.; Osa, S.; Matsumoto, N.; Iijima, S.; Sunatsuki, Y.; Kojima, M.; Dahan, F.; Tuchagues, J.-P. *Inorg. Chem.* **2003**, *42*, 7001−7017.
(17) Hayami, S.; Gu, Z.-Z.; Einaga, Y.; Kobayashi, Y.; Ishikawa, Y.; Yamada, Y.; Fujishima, A.; Sato, O. *Inorg. Chem.* **2001**, *40*, 3240−3242.
(18) Bonhommeau, S.; Guillon, T.; Daku, L. M. L.; Demont, P.; Costa, J. S.; Létard, J.-F.; Molnar, G.; Bousseksou, A. *Angew. Chem., Int. Ed.* **2006**, *45*, 1625−1629.
(19) Guionneau, P.; Gac, F. L.; Kaiba, A.; Costa, J. S.; Chasseau, D.; Létard, J.-F. *Chem. Commun.* **2007**, 3723−3725.
(20) Roux, C.; Zarembowitch, J.; Gallois, B.; Granier, T.; Claude, R. *Inorg. Chem.* **1994**, *33*, 2273−2279.
(21) Hasegawa, Y.; Kume, S.; Nishihara, H. *Dalton Trans.* **2009**, 280−284.
(22) Boillot, M.-L.; Chantraine, S.; Zarembowitch, J.; Lallemand, J.-Y.; Prunet, J. *New. J. Chem.* **1999**, 179−183.
(23) Boillot, M.-L.; Pillet, S.; Rivière, E.; Claiser, N.; Lecomte, C. *Inorg. Chem.* **2009**, *48*, 4729−4736.
(24) Sénéchal-David, K.; Zaman, N.; Walko, M.; Halza, E.; Rivière, E.; Guillot, R.; Feringa, B. L.; Boillot, M.-L. *Dalton Trans.* **2008**, 1932−1936.
(25) Tissot, A.; Boillot, M.-L.; Pillet, S.; Codjovi, E.; Boukheddaden, K.; Daku, L. M. L. *J. Phys. Chem. C* **2010**, *114*, 21715−21722.
(26) Hasegawa, Y.; Takahashi, K.; Kume, S.; Nishihara, H. *Chem. Commun.* **2011**, *47*, 6846−6848.
(27) Holland, J. M.; McAllister, J. A.; Lu, Z.; Kilner, C. A.; Thornton-Pett, M.; Halcrow, M. A. *Chem. Commun.* **2001**, 577−578.
(28) Tweedle, M. F.; Wilson, L. J. *J. Am. Chem. Soc.* **1976**, *98*, 4824−4834.
(29) Nakano, K.; Suemura, N.; Yoneda, K.; Kawata, S.; Kaizaki, S. *Dalton Trans.* **2005**, 740−743.
(30) Dupouy, G.; Marchivie, M.; Triki, S.; Sala-P., J.; Salaün, J.-Y.; Gómez-G., C. J.; Guionneau, P. *Inorg. Chem.* **2008**, *47*, 8921−8931.
(31) Marconi, G.; Bartocci, G.; Mazzucato, U.; Spalletti, A.; Abbate, F.; Angeloni, L.; Castellucci, E. *Chem. Phys.* **1995**, *196*, 383−393.
(32) Toftlund, H. *Coord. Chem. Rev.* **1989**, *94*, 67−108.
(33) Bree, A.; Zwarich, R. *J. Mol. Struct.* **1981**, *75*, 213−224.
(34) Hamaguchi, H.; Iwata, K. *Bull. Chem. Soc. Jpn.* **2002**, *75*, 883−897.
(35) Johnson, C. S.; Chang, R. *J. Chem. Phys.* **1965**, *43*, 3183−3192.
(36) Happ, J. W.; Ferguson, A.; Whitten, D. G. *J. Org. Chem.* **1972**, *37*, 1485−1491.
(37) Kobatake, S.; Hasegawa, H.; Miyamura, K. *Cryst. Growth Des.* **2011**, *11*, 1223−1229.
(38) Evans, D. F. *J. Chem. Soc.* **1959**, 2003−2005.
(39) Hansch, C.; Leo, A.; Taft, R. W. *Chem. Rev.* **1991**, *91*, 165−195.
(40) Wu, D.-Y.; Sato, O.; Einaga, Y.; Duan, C.-Y. *Angew. Chem., Int. Ed.* **2009**, *48*, 1475−1478.
(41) Kitchen, J. A.; Jameson, G. N. L.; Tallon, J. L.; Brooker, S. *Chem. Commun.* **2010**, *46*, 3200−3202.
(42) Holland, J. M.; McAllister, J. A.; Kilner, C. A.; Thornton-Pett, M.; Bridgeman, A. J.; Halcrow, M. A. *J. Chem. Soc., Dalton Trans.* **2002**, 548−554.
(43) Carbonera, C.; Costa, J. S.; Money., V. A.; Elhaïk, J.; Howard, J. A. K.; Halcrow, M. A.; Létard, J.-F. *Dalton Trans.* **2006**, 3058−3066.
(44) Nihei, M.; Han, L.; Oshio, H. *J. Am. Chem. Soc.* **2007**, *129*, 5312−5313.
(45) Rajadurai., C.; Qu, Z.; Fuhr, O.; Gopalan, B.; Kruk, R.; Ghafari, M.; Ruben, M. *Dalton Trans.* **2007**, 3531−3537.
(46) Guionneau, P.; Marchivie, M.; Bravic, G.; Létard, J.-F.; Chasseau, D. *J. Mater. Chem.* **2002**, *12*, 2546−2551.
(47) Halcrow, M. A. *Chem. Soc. Rev.* **2011**, *40*, 4119−4142.
(48) Hostettler, M.; Törnroos, K. W.; Chernyshov, D.; Vangdal, B.; Bürgi, H.-B. *Angew. Chem., Int. Ed.* **2004**, *43*, 4589−4594.
(49) Elhaïk, J.; Pask, C. M.; Kilner, C. A.; Halcrow, M. A. *Tetrahedron* **2007**, *63*, 291−298.
(50) Chandrasekar, R.; Frank, F.; Susan, B.; Olaf, F.; Mohamed, G.; Robert, K.; Mario, R. *Inorg. Chem.* **2006**, *45*, 10019−10021.
(51) Jaganathan, S.; Tsukamoto, M.; Schlosser, M. *Synthesis* **1990**, 109−111.
(52) Tsukamoto, M.; Schlosser, M. *Synlett* **1990**, 605−608.
(53) Terent'eva, A. A.; Krumgal'z, B. S.; Gerzhberg, Y. I. *Zh. Prkl. Khim.* **1973**, *56*, 1143−1144.
(54) Altomare, A.; Cascarano, G.; Guagliardi, A.; Burla, M. C.; Polidori, G.; Camalli, M. *J. Appl. Crystallogr.* **1994**, *27*, 435−436.
(55) Sheldrick, G. M. *SHELX-97, Programs for Crystal Structure Analysis* (Release 97-2); University of Göttingen: Göttingen, Germany, 1997.
(56) Farrugia, L. J. *J. Appl. Crystallogr.* **1999**, *32*, 837−838 (an integrated system of Windows programs for the solution, refinement, and analysis of single-crystal X-ray diffraction data).